Area dependent efficiency of organic solar cells

Dhritiman Gupta, Monojit Bag, and K. S. Narayan

Citation: Applied Physics Letters **93**, 163301 (2008); doi: 10.1063/1.2998540
View online: http://dx.doi.org/10.1063/1.2998540
View Table of Contents: http://scitation.aip.org/content/aip/journal/apl/93/16?ver=pdfcov
Published by the AIP Publishing

Area dependent efficiency of organic solar cells

Dhritiman Gupta, Monojit Bag, and K. S. Narayan[a)]
Jawaharlal Nehru Centre for Advanced Scientific Research, Jakkur P. O. Bangalore, Karnataka 560064, India

(Received 4 August 2008; accepted 19 September 2008; published online 20 October 2008)

Efficiency estimations of organic solar cells are observed to be dependent on the dimensions of electrode defining the active area. We address this issue and explore the manner in which efficiency scales in polymer solar cells by studying these devices as a function of electrode area and incident beam size. The increase in efficiency for smaller active areas can be explained by the reduced electrical resistive loss, the enhanced optical effects, and the finite additional fraction of photogenerated carriers in the vicinity of the perimeter defined by the metal electrode © *2008 American Institute of Physics*. [DOI: 10.1063/1.2998540]

Organic solar cells are intensely being studied as a potential photovoltaic (PV) device due to the solution processing methods and the relative ease in fabrication. The combination of unique semiconducting electronic property and mechanical aspects similar to conventional plastics is an attractive feature in spite of the lower efficiencies prevailing in these systems. The increasing number of reports necessitates accurate estimation of power conversion efficiency (η) and appropriate comparison of devices with a uniform set of guidelines for the parameters, especially with regard to the dimensions of the PV element and the extrapolation procedures of the parameters to large area pixelated structures.[1,2]

The basic active ingredients for the polymer solar cells (PSCs) are widely used donor and acceptor kind of polymers intermixed to form bulk-heterojunction (BHJ) facilitating charge transfer and transport processes. In a BHJ-PSC based on poly(3-hexylthiophene) (P3HT) and [6,6]-phenyl-C_{61}-butyric acid methyl ester (PCBM), η has reached up to 5%,[3,4] including a recent report of $\eta \approx 6\%$ in solution-processed PSCs in a tandem cell geometry.[5] In BHJ-PSCs, efforts have largely been targeted to optimize the bulk morphology for efficient charge generation and subsequent transport.[4] Recent efforts have also addressed the role of cathode-polymer interface in determining the fill factor of solar cells.[6,7] However, efforts in optimizing the geometry and pixel dimensions and distribution have been quite negligible. A small active area (typically <10 mm^2), defined by the overlap area of the bottom indium tin oxide (ITO) anode and the top cathode, has been reported to give rise to high short-circuit current density (J_{SC}) values.[8] We highlight the importance of the cathode size and the extent of photoactive regions beyond the assumed dimensions in PSCs. This issue has been partly addressed in an earlier report for organic PV devices;[9,10] however, we present additional insights and observations which can potentially be utilized to design an effective grid pattern for a large area polymer PV structure.

For the present studies, P3HT-PCBM based PSCs were fabricated using standard protocol by spin coating the polymer solution onto poly(ethylenedioxythiophene):poly(styrene sulfonic acid) (PEDOT-PSS) coated, unpatterned, ITO-glass substrates. Devices of wide range of active area $A \approx 0.01-1$ cm^2 were prepared by metal deposition onto the active polymer layer of P3HT:PCBM. Shadow mask arrangements were used to pattern accurate predefined square electrodes on the active layer with asymmetry factors (cathode area /ITO area) ranging from 10^{-3} to 10^{-1}.

These devices were tested under complete illumination using collimated white light source. η of $\sim 2\%$ was achieved for a prototypical device under AM1.5 illumination. We chose a batch of devices for the present studies which represented a slightly lower η but which could be reliably reproduced. The J (current/cathode area)-V (Fig. 1) for these representative devices indicates J_{SC} in the range of 2.68 mA/cm^2($\eta \approx 0.9\%$)–1.42 mA/cm^2($\eta \approx 0.48\%$). In all the batches, a general trend of reproducible high J_{SC} value for small-area devices was observed (S1 in Ref. 11). The decay of J_{SC} for different area devices in general follows a $1/x$ ($\approx$perimeter/A of the cathode) decay profile where x is the square-cathode dimension (Fig. 1), while V_{OC} was relatively unaffected. The enhancement of J with decreasing area can be expressed as $J_0[1+1/(kA)]$, k: constant, in the range studied.

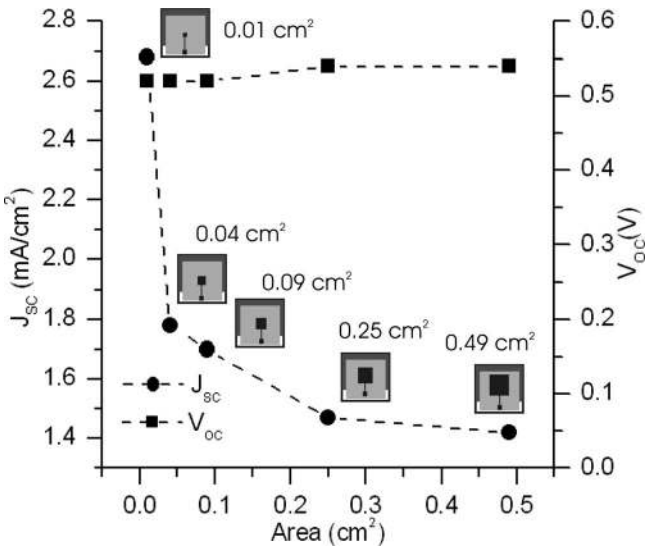

FIG. 1. Variation in J_{SC} and V_{OC} with different active areas for a P3HT-PCBM solar cell under flooded white light illumination of intensity ~ 80 mW/cm^2. Devices were fabricated on two different substrates with pixel sizes of 0.01, 0.04, and 0.09 cm^2 (substrate 1), and 0.25 and 0.49 cm^2 (substrate 2). The schematic diagram of the different active area devices is depicted in the inset.

a)Electronic mail: narayan@jncasr.ac.in.

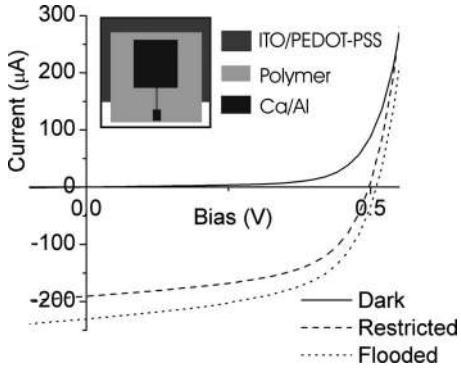

FIG. 2. The *J-V* characteristics of 0.25 cm^2 device under flooded and restricted collimated illumination using a calibrated 50 mW/cm^2 Xe source. The device layout has been depicted in the inset.

Experiments were then carried out to estimate the significant apparent contribution from the nonoverlapping region. For this, the devices were characterized using restricted illumination by inserting a mask which precisely fitted the active region and covered the peripheral regions. The metal-cathode contour was used for mask alignment while maintaining negligible shadow effects. The measurements in all the cases indicated a substantial drop in I_{SC} (by ~15% for the 0.25 cm^2 device) as compared to the flooded illumination, which also illuminated the peripheral regions around the active region (Fig. 2). Under restricted illumination, the *J-V* characteristics for different area devices are identical and superpose on each other, revealing that resistive losses are not a dominant factor in the present range of devices. The finite drop across the ITO surface (between the electrical contact point and the region of illumination) barely accounts for these significant changes. Since the ITO is not patterned, contributions from the PEDOT-PSS (resistivity ~0.1 Ω cm) layer are not relevant here.

Possible sources of the contribution from the periphery are expected to arise from the diffused component of light scattered due to the surface roughness of the ITO/polymer interface. This contribution can be quantitatively addressed in terms of the haze parameter for the transmitted light (H_T) [the ratio between diffused and total (diffused+specular) light]. H_T depends on the substrate root-mean-square surface roughness (Λ) and incident wavelength λ with larger contribution from shorter λ. It is an appreciable factor at visible region when Λ exceeds 40–50 nm.[12] For λ≈530 nm (absorption here if possible maximum), the H_T has been shown to be only 15% and gives rise to negligible enhancement in J_{SC} considering Λ≈1 nm for ITO/PEDOT and Λ ≈1.37 nm for Al/polymer interface. Beam spreading within the glass substrate (thickness ~1.12 mm, refractive index ≈1.45) is a sizable factor under nonuniform illumination conditions. The optical effects arising from the glass substrate were verified by using thinner substrates such as ITO coated cover-slip glass (thickness ~160 μm). Devices fabricated on these thinner substrates exhibited similar performance levels. Measurements involving restricted illumination indicated small contributions from the periphery in this case. The light distribution in the polymer medium was simulated using Fourier optics numerical simulation tools (S3 in Ref. 11), and was also verified experimentally by studying the extent of the beam spread using a near-field collection setup around the edges upon irradiating the sample in the far field. Direct images of the scattered light from the device using a high resolution camera also provided the intensity profiles. A small spot of light (spot size ~200 μm) was focused on the ITO through a 50× objective lens and the scattered intensity profile was captured from the other side with a charge coupled device camera. For a localized incident spot the scattering factors in the cover slips (160 μm) are 30% less than those in glass slides (1.15 mm). Consequently, the enhancement of J_{SC} from the additional peripheral illumination using a well collimated source is ≈5% in the case of cover slips as compared to 15% in the case of glass substrates for similar area devices. These effects have been observed to be more pronounced in the case of the results from small-area illumination on a dye-sensitized solar cell on much thicker (4 mm) substrates.[13] The possibility of efficient guiding of isotropically re-emitted light by the absorbing polymer species,[14] coated on glass substrates, is not significant from these low emission systems.

Finite extent of the fringing electric field outside the coverage of the Al cathode was estimated to decay to magnitudes of as low as ~10–100 V/cm within a span of 50 nm from the edge. The extent of photoactive region outside the active area was probed locally using spatially resolved I_{SC} measurements with a low intensity (~120 nW) source incident using a 60× microscope objective (λ~470 nm, spot size ~1 μm) (S2 in Ref. 11) and a stage translated at a step size of 0.5 μm. Measures were taken to minimize the diffusive spreading of light and minimize wave guiding by fabricating the devices on thin ITO coated cover slip (160 μm). The short-circuit-photocurrent (I_{ph}) decreases progressively as the light is scanned away from the overlap region of the electrodes.[15] The I_{ph} decay profiles (corrected with transmission profile) outside the Al electrode and ITO electrode reveal decay lengths of 16 and 109 μm, respectively [Fig. 3(a)].[16] It is to be noted that the I_{ph} from these measurements have their origin from the localized source of carrier generated by the narrow light source that distorts the built-in potential locally. In the steady state, a nonlocal lateral electric field can be set up that can self-consistently induce a lateral flow of the separated carriers. This lateral charge flow, which is Ohmic in nature, produces a potential drop between the locus of illumination, and the electrodes can be used to possibly explain the large decay lengths beyond the expected value for simple diffusion processes.[15]

Measurements with two beams on the two regions (within the device area and outside the device) are more appropriate to confirm the processes under broad uniform illumination. These were carried out with two light sources [schematic in Fig. 3(b)] on a solar cell device fabricated on a smooth thin ITO coated cover-slip substrate to minimize the beam dispersion. One source was directed from the ITO side onto the overlapping region in front of the Al while the second beam was incident from the opposite side, with the light focused on the region outside the Al region. A clear increase in the J_{SC} was observed when the second source was incident outside the overlapping region; however, this increase was less than the sum of the values obtained from individual contributions. This expected nonadditive feature can be understood from the differences in the charge carrier transport rate from the two carrier generation sources. The lateral diffusion process rates assisted by small field are expected to be

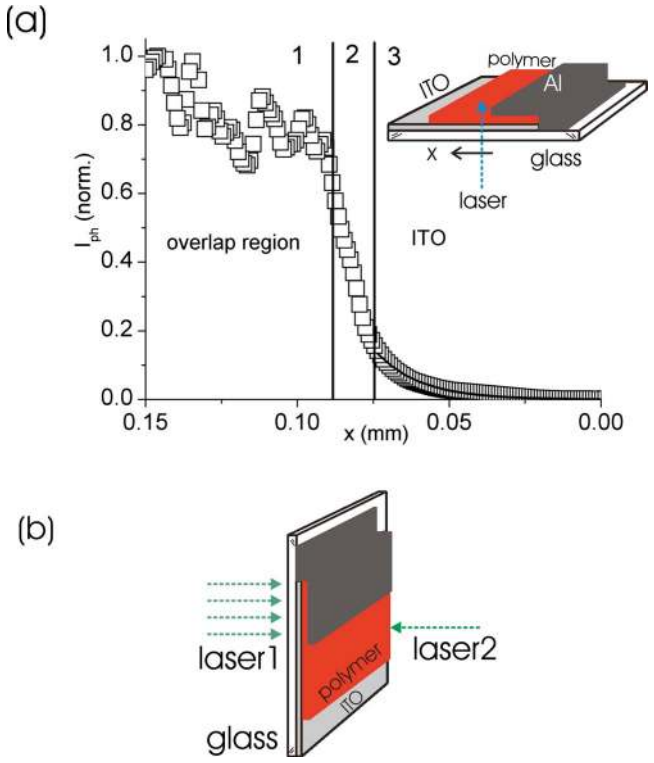

FIG. 3. (Color online) (a) Spatially resolved short-circuit photocurrent (I_{ph}) profile of a BHJ solar cell made from P3HT-PCBM blend sandwiched between unpatterned ITO and a stripe of Al cathode. The transmission of the beam was monitored using a photodetector to determine the position of the beam. In region 1, the spot (1 μm diameter) is completely inside the overlap region. Region 2 corresponds to the boundary region where edge effects dominate. In region 3, the spot is completely outside and the transmission is position independent. The exponential fit (solid line) to the data reveals the decay length of 16 μm. Inset depicts the device structure and the schematic of the measurement. The long arrow indicates scanning direction. (b) I_{ph} measurement using two beams with broad illumination restricted within the overlap region and a local point source illumination in the external region.

lower than the transverse transport rates aided by the large built-in field. This feature is also evidenced in the transient J_{SC} profiles from the carriers generated at the two locations. The beam size dependence was also observed to be markedly less sensitive for smaller A devices; the beam concentrated in a small area of diameter 485 μm gave rise to the J_{SC} which differs only by $<2\%$ as compared to a larger spot (0.025 cm^2) falling on the overlap region of a 0.01 cm^2 device.

Earlier reports on area scaling basically dealt around the issues of the finite sheet resistance of ITO anode which give rise to a finite loss in efficiency due to I^2R drop.[17,18] The total power loss P_{loss} is given by $P_{loss}=J^2R_{sheet}bL^3/24$, where J is the current density, R_{sheet} ($\sim 10\ \Omega/\square$) is the sheet resistivity of the ITO, b is the width, and L is the spacing between two metallic grid lines on the ITO slab.[19] In order to circumvent the ITO sheet resistance drop, the area of the device was required to be <1 cm^2 since for a 5% efficient solar cell (area=1 cm^2, $J_{SC}=13$ mA/cm^2, $V_{OC}=0.6$ V, $FF=0.65$, $J_{max}=10$ mA/cm^2, and $V_{max}=0.5$ V) the fractional power loss $[p=\text{Ploss/power generated at maximum power point}]/P_{loss}=J_{max}R_{sheet}L^2/(12V_{max})$ is $\approx 16\%$. Our present results suggest the benefits of further pixelation within this 1 cm^2 area of the metal cathode. The possible enhancement of the total power efficiency $\eta_{pixel}/\eta_{nonpixel}$ of a large area device upon cathode patterning can be quantified by a scaling argument and can be expressed as $(1+b)/(1+c)$, where $(1+b)$ is the gain factor from $J_{pixel}/J_{nonpixel}$ and $(1+c)$ corresponds to $(A_{nonpixel}/nA_{pixel})$ factor, where c quantifies the effective reduced photon incident area upon pixelation of the structure. The observation of the enhanced J with decreasing A can more than compensate the decrease arising from this reduced A. The enhancement factor b is expected to be dependent on c, thereby posing a limit. The cathode pixelation which can be accomplished with various methods can enable the device to utilize the higher efficiencies observed in smaller area device, which can more than compensate the loss arising from a decreased net active area.

In conclusion, we have demonstrated contributions from the optical and electrical effects to the area dependence of η in PSCs. Besides emphasizing the need for standardizing PSCs for evaluation and comparison purposes, we suggest the possibility of constructing a hierarchy in the patterns, where the ITO is patterned at a larger length scale and cathodes are patterned at smaller levels, to enable extraction of high levels of performance from these structures.

K.S.N. acknowledges the Department of Science and Technology for partially funding the project.

[1] G. P. Smestad, F. C. Krebs, C. G. Lampert, C. G. Granqvist, K. L. Chopra, X. Mathew, and H. Takakura, Sol. Energy Mater. Sol. Cells **92**, 371 (2008).
[2] V. Shrotriya, G. Li, Y. Yao, T. Moriarty, K. Emery, and Y. Yang, Adv. Funct. Mater. **16**, 2016 (2006).
[3] M. Reyes-Reyes, K. Kim, and D. L. Carroll, Appl. Phys. Lett. **87**, 083506 (2005).
[4] G. Li, V. Shrotriya, J. Huang, Y. Yao, T. Moriatry, K. Emery, and Y. Yang, Nat. Mater. **4**, 854 (2005).
[5] J. Y. Kim, K. Lee, N. E. Coates, D. Moses, T.-Q. Nguyen, M. Dante, and A. J. Heeger, Science **13**, 222 (2007).
[6] D. Gupta, M. Bag, and K. S. Narayan, Appl. Phys. Lett. **92**, 093301 (2008).
[7] D. Gupta, S. Mukhopadhyay, and K. S. Narayan (in press).
[8] D. L. Carroll, J. Jiu, M. Namboothiry, and K. Kim, Appl. Phys. Lett. **91**, 266102 (2007).
[9] A. Cravino, P. Schilinsky, and C. J. Brabec, Adv. Funct. Mater. **17**, 3906 (2007).
[10] M. Kim, M.-G. Kang, L. J. Guo, and J. Kim, Appl. Phys. Lett. **92**, 133301 (2008).
[11] See E-APPLAB-93-040841 for additional experimental details. This document can be reached via the EPAPS homepage (http://www.aip.org/pubservs/epaps.html).
[12] J. Krc, M. Zeman, F. Smole, and M. Topic, J. Appl. Phys. **92**, 749 (2002).
[13] S. Ito, Md. K. Nazeeruddin, P. Liska, P. Comte, R. Charvet, P. Pechy, M. Jirousek, A. Kay, S. M. Zakeeruddin, and M. Gratzel, Prog. Photovoltaics **14**, 589 (2006).
[14] M. J. Currie, J. K. Mapel, T. D. Heidel, S. Goffri, and M. A. Baldo, Science **321**, 226 (2008).
[15] D. Kabra and K. S. Narayan, Adv. Mater. (Weinheim, Ger.) **19**, 1465 (2007).
[16] The spatially resolved photocurrent with the beam scanning the Al electrode track (outside the ITO boundary) also reveals an exponential type decay profile.
[17] A. K. Pandey, J. M. Nunzi, B. Raiter, and A. Moliton, Phys. Lett. A **372**, 1333 (2008).
[18] C. Lungenschmied, G. Dennler, H. Neugebauer, S. N. Sariciftci, M. Glatthaar, T. Meyer, and A. Meyer, Sol. Energy Mater. Sol. Cells **91**, 379 (2007).
[19] M. A. Green, *Solar Cells, Operating Principles, Technology and System Applications* (University of New South Wales, Kensinfton, 1998).